Title
Role of atomic coordination on superconducting properties of boron-doped amorphous carbon

Journal
Physical Review Materials, 3(8)

ISSN
2476-0455

Authors
Sakai, Yuki
Chelikowsky, James R
Cohen, Marvin L

Publication Date
2019-08-01

DOI
10.1103/physrevmaterials.3.084802

Peer reviewed

Role of atomic coordination on superconducting properties of boron-doped amorphous carbon

Yuki Sakai,[1] James R. Chelikowsky,[1,2,3] and Marvin L. Cohen[4,5]

[1]*Center for Computational Materials, Oden Institute for Computational Engineering and Sciences, The University of Texas at Austin, Austin, Texas 78712, USA*

[2]*Department of Chemical Engineering, The University of Texas at Austin, Austin, Texas 78712, USA*

[3]*Department of Physics, The University of Texas at Austin, Austin, Texas 78712, USA*

[4]*Department of Physics, University of California at Berkeley, Berkeley, California 94720, USA*

[5]*Materials Sciences Division, Lawrence Berkeley National Laboratory, Berkeley, California 94720, USA*

(Dated: May 6, 2019)

Abstract

We study the effect of atomic coordination (orbital hybridization) on superconducting properties of boron-doped amorphous carbon. The ratio of three-fold coordinated (sp^2-hybridized) and four-fold coordinated (sp^3-hybridized) atoms in the system is found to have an impact on their electronic, vibrational and superconducting properties. Our findings show that a high proportion of four-fold coordination in both carbon and boron atoms are important for realizing a high superconducting transition temperature.

I. INTRODUCTION

The competing configuration between an sp^2 and an sp^3 orbital hybridization in carbon atoms causes diverse carbon allotropes. Both sp^2 and sp^3 carbon allotropes are known to become superconductors when boron atoms (i.e., holes) are incorporated into their structures. For example, diamond is completely composed of sp^3-coordinated carbon atoms and exhibits superconductivity when carbon atoms are replaced with boron atoms, owing to shallow acceptor states created by boron doping [1–3]. Carbon nanotubes where carbon atoms are sp^2-hybridized also become superconducting when the Fermi energy is tuned to be close to the van Hove singularity in the density of states by hole doping [4, 5]. Fullerene crystals and graphite become superconductors when alkali atoms are doped into their empty spaces [6, 7]. Recent report on twisted bilayer graphene shows superconductivity at some magic twist angles even without a carrier doping [8].

Amorphous carbon has an interesting structural property wherein both sp^2 (three-fold) and sp^3 (four-fold) hybridized carbon atoms are randomly distributed. Recently, a new amorphous (disordered) carbon structure, *Q-carbon*, was reported to have various interesting properties such as ferromagnetism and super-hardness [9, 10]. Q-carbon exhibits superconductivity when doped with boron [10, 11]. The reported superconducting transition temperatures (T_c) are 36 K and 55 K for boron doping concentration of 17% and 25%, which are significantly higher than those reported on boron-doped diamond (11 K) and carbon nanotubes (19 K under pressure) [1–5]. The reported T_c for the Q-carbon is higher than that of MgB_2 (39 K) [12]. A theoretical study showed that the shallow acceptor states created by boron doping is important and the estimated T_c is 37 K at 14% doping concentration in amorphous carbon [13]. The proportion of four-fold atoms in the theoretical structure (81%) agrees with the experimentally observed value (approximately 85 %) [11]. Although the predicted T_c and the percent of four-fold coordination is consistent with the earlier experimental report, the simulation was performed only on a single mass density (3.4 g/cm^3) and only on a few different amorphous structures. More detailed studies are required as the structural information from experiments remains limited to the proportion of three-fold and four-fold atoms.

Here we examine the superconducting properties of boron-doped amorphous carbon with various mass densities and structures. We obtain superconducting parameters for boron-

doped amorphous carbon with initial (before boron doping) mass densities from 2.5 to 4.5 g/cm^3. The mass density affects the superconducting properties through their different proportions of three-fold and four-fold coordinated carbon atoms. The mass density also affects the phonon modes in amorphous carbon. A high density above diamond results in short covalent bond lengths and induces a blueshift of phonon frequencies. These different three-fold:four-fold ratio and stiffening of the phonon modes support a high superconducting transition temperature in a high-density boron-doped amorphous carbon. Consequently, the superconducting transition temperature generally increases as a function of the mass density.

II. COMPUTATIONAL METHOD

A total energy real-space pseudopotential approach with Troullier-Martins pseudopotentials [14–16] constructed within density functional theory is employed using the local density approximation for the exchange-correlation functional [17–20]. A real-space grid of 0.3 Bohr (1 Bohr = 0.52918 Å) and a plane-wave energy cutoff of 65 Ry (1 Ry = 13.606 eV) are used to obtain sufficiently converged results. A k-grid of $2 \times 2 \times 2$ is used for a Brillouin-zone integration.

The real-space pseudopotential first-principles code PARSEC is used for molecular dynamics (MD) simulations [21–24]. MD simulations are performed to obtain an initial model structure of undoped amorphous carbon. First we prepare a 64 carbon atoms supercell in a simple cubic structure. Next we perform MD simulation at 7500 K under a constant volume and temperature to randomize the atomic coordinates. The system temperature is controlled by using stochastic Langevin thermostat with a friction constant of 10^{-3} a.u [25]. A time step of 1 fs is used for the MD simulations.

Phonon modes are computed at the Γ point by using density functional perturbation theory [26, 27]. We also compute the electron-phonon linewidth of each phonon mode from electron-phonon matrix elements [28]. In that case, we take a denser k-grid of 6×6×6 for a Brillouin zone integration to perform a more accurate calculation. A Gaussian broadening of 0.015 to 0.025 Ry is used to obtain converged superconducting parameters. The Eliashberg spectral function is computed from the linewidth and used to estimate the electron-phonon coupling strength λ. The superconducting transition temperature is estimated from λ by

using Allen-Dynes modified version of McMillan equation

$$T_c = \frac{\omega_{\log}}{1.2} \exp\left[\frac{-1.04(1+\lambda)}{\lambda(1-0.62\mu^*)-\mu^*}\right], \tag{1}$$

with an effective Coulomb repulsion parameter μ^* of 0.12 [29]. Here $\omega_{\log}$ is the logarithmic average of phonon frequency defined by

$$T_c = \exp\left[\frac{2}{\lambda}\int d\omega \frac{\alpha^2(\omega)}{\omega}\ln(\omega)\right]. \tag{2}$$

III. INITIAL AMORPHOUS STRUCTURE AND BORON SUBSTITUTION

Generating amorphous structures from a boron-carbon mixture generally fails to obtain shallow acceptor states and results in deep localized states [13]. A more reliable method to obtain shallow acceptor states is first preparing an initial undoped amorphous structure and then replacing carbon atoms with boron atoms. Our goal is to obtain a structure of boron-doped amorphous carbon that is promising for high temperature superconductivity, i.e., one that possesses shallow acceptor states. Therefore, we intentionally choose a substitutional site which optimizes not the total energy but the electronic structure. We select two initial amorphous carbon structures with completely different electronic structures for each density to consider the effect of the initial condition for substitutional doping. Here one initial structure has less localized states, which is generally ideal for the superconductivity. The other structure has non-ideal electronic structure where several deep localized states already exist without boron doping.

The two leftmost data sets in Fig. 1 show the Kohn-Sham energy eigenvalues around the highest occupied (128th) state of two undoped amorphous carbon structures. The data labeled as "Localized" exhibits four (from 125 to 128th) states with localized nature. The third highest occupied states (blue squares) have 1.5 eV above the reference energy [we take the mean value ($\bar{\epsilon}$) of 120th eigenvalues at eight k points on a 2×2×2 grid as this reference]. Thus this initial structure should not be ideal for obtaining shallow acceptor states. On the other hand, the second highest energy states of the data labeled "0" is less than 1.5 eV and only the highest energy state is localized. This electronic structure should be a more suitable starting point for the superconductivity.

A substitutional boron doping to amorphous carbon typically results in a complicated structural modification around the substitutional site. The resultant electronic structure

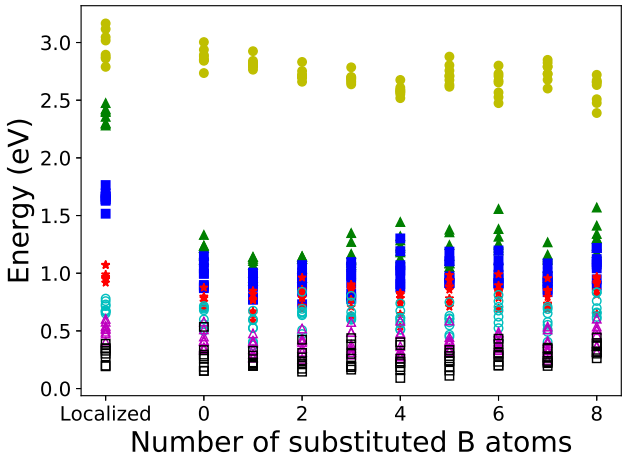

FIG. 1. (Color online) Kohn-Sham eigenvalues of amorphous carbon with the initial mass density of 3.5 g/cm^3 as a function of the number of substituted boron atoms up to eight. Filled yellow circles, green triangles, blue squares, and red stars represent 128th, 127th, 126th, and 125th eigenvalues, respectively. Open sky blue circles, cyan triangles, and black squares indicate 124th, 123rd, and 122nd eigenvalues, respectively.The eigenvalues are measured from a reference energy ($\bar{\epsilon}$) which is the mean value of eight 120th eigenvalues. For a comparison, a more localized eigenvalue of undoped amorphous carbon is also represented at the leftmost column of the figure.

strongly depends on the substitutional sites. We perform substitutional doping in the following way: (1) Substitutionally dope 64 sites with B atom and relax the structure (2) Determine a substitutional site so that the number of localized states are as small as possible. To achieve this, we first define a reference eigenstate energy (120th state here). Then we compute the energy differences between the reference energy and other eigenvalue energies of several electronic states (121st to 128th states, which are supposed to be or be near acceptor states upon boron doping). We use the energy differences as a measure of the shallowness of those impurity states. Here we do not chose a substitutional site that is based on the lowest total energy. (3) Substitutional doping to 63 remaining sites and determine another doping site. (4) Repeat the same decision process until eight boron atoms are doped into the system.

Figure 1 shows the evolution of Kohn-Sham eigenvalue energies with respect to boron doping. Here we select the substitutional site by the above criterion. The initial (undoped) electronic structure shows a deep localized state which arises from a three-fold coordinated

carbon atoms surrounded by four-fold coordinated atoms. The eigenvalues are not necessarily lowered upon the boron doping but the doping does not strongly modify the original electronic structure and does not create additional localized states. We take a fixed value of 12.5% ("8" in Fig. 1) as the boron concentration of amorphous carbon with various densities for a comparison purpose.

IV. RESULTS AND DISCUSSIONS

Table I lists the superconducting parameters of 12.5% boron-doped amorphous carbon with different initial mass densities and structures. A structure is named by its initial mass density and initial structure (see the previous section for the different initial structures). For example, 3.5(N) represent that its initial structure is non-ideal and the initial mass density is 3.5 g/cm^3. The two rows show similar superconducting transition temperatures T_c for the boron-doped amorphous carbon with the initial densities of 2.5, 3.5, and 4.5 g/cm^3 as the difference in T_c is less than or equal to 5 K. Those with the initial densities of 3.0 and 4.0 g/cm^3 shows a larger deviation than 10 K. In such cases, the densities of states at the Fermi level have notable differences [11.4 and 15.2 states/spin/Ry/cell, in the 3.0 and 4.0 g/cm^3 cases, respectively]. A larger density of states at the Fermi energy results in a higher T_c when the density is the same. The initial structure has a non-negligible effect on the T_c under the current procedure of constructing a model of boron-doped amorphous carbon. However, there is no strong-correlation between the initial electronic structure and the superconducting properties as an amorphous structure is easily changed by substitutional doping.

The general trend seen from Table I is that electron-phonon coupling strength λ and T_c increases as a function of mass density. However, the lowest-density case 2.5(I) shows significantly large λ (1.46) but the T_c is not high (15.4 K) because this sizable λ arises from a low frequency mode. The contribution from such a low frequency mode does not contribute to T_c as the logarithmic average frequency $\omega_{\log}$ is suppressed (see Eqs. 1 and 2). In fact, the λ and $\omega_{\log}$ becomes 0.68 and 427 cm^{-1}, respectively when the contribution from the lowest-frequency optical mode is excluded. The T_c is not significantly affected (11.5 K) by the exclusion of this mode.

Figure 2 represents the radial distribution functions of boron-doped amorphous carbon

TABLE I. Superconducting parameters of 12.5% boron-doped amorphous carbon with various initial densities (g/cm^3) and structures. Electron-phonon coupling strength λ, logarithmic average frequency $\omega_{\log}$ (cm^{-1}), density of states at Fermi energy $N(E_F)$ (states/spin/Ry/cell), superconducting transition temperature T_c (K), and sp^3 (or four-fold coordination) proportion (%) are listed. The name of the structure represent the initial mass density (g/cm^3) and the two initial amorphous carbon structure: ideal (I) or non-ideal (N) structures, respectively.

Structure	λ	$\omega_{\log}$	$N(E_F)$	T_c	sp^3 proportion
2.5(I)	1.46	148	87.0	15.4	31.2
2.5(N)	0.62	495	87.6	10.4	34.4
3.0(I)	0.82	520	78.2	22.4	65.6
3.0(N)	1.03	527	89.6	34.8	71.9
3.5(I)	0.79	689	70.1	27.4	87.5
3.5(N)	1.00	513	70.1	32.1	93.8
4.0(I)	1.14	488	67.2	37.5	96.8
4.0(N)	0.80	565	52.0	23.3	90.6
4.5(I)	1.00	539	54.5	34.3	93.8
4.5(N)	1.24	438	52.0	37.9	92.2

with different densities. The first peak is located close to the sp^2 bond length of carbon (1.42 Å) at the low density case [2.5(I), green solid line], reflecting the tendency that low density amorphous carbon prefers sp^2 hybridization [30]. The first peak shifts toward the sp^3 bond length (1.54 Å) when the density is close to the diamond density [3.5(N), red dashed line]. However, the first peak again shifts toward small distance in the higher density case [4.5(N), blue dash-dotted line]. Here the peak becomes close to the sp^2 bond length because of the high density beyond that of diamond. Interestingly the second peak is shifted toward the short distance region as we increase the density. This indicates the second nearest-neighbor distances is also decreased because of the compressed cell.

We consider the effect of mass density and orbital hybridization by looking at the density of states projected onto atoms. Figure 3 shows the total and projected electronic density of states of boron-doped amorphous carbon. The low-density 2.5(I) structure contains sizable amounts of three-fold atoms (about 66 %, see Table I). This causes a considerable contribu-

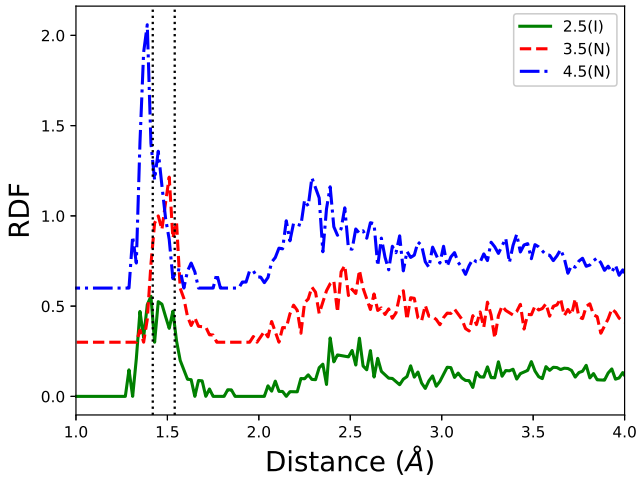

FIG. 2. (Color online) Radial distribution functions (RDF) of 12.5% boron-doped amorphous carbon. Green solid, red dashed, and blue dash-dotted curves represent the distribution functions of 2.5(I), 3.5(N), and 4.5(N) cases, respectively. Curves are shifted to separate from each other. The two vertical black dotted lines indicate the typical bond lengths of sp^2 (1.42 Å) and sp^3 (1.54 Å) hybridized carbon atoms.

tion from the three-fold atoms to the electronic states around the Fermi energy as shown in the red dashed line in Fig. 3(a). On the other hand, there is virtually no contribution from three-fold coordinated atoms in higher density cases such as 3.5(N), 4.0(I), and 4.5(N) [see Figs. 3(d), 3(e), and 3(f)]. As listed in Table I, the T_c of the low-density 2.5(I) structure (15.4 K) is significantly lower than the three high-density cases although the density of states at the Fermi energy (87.0 states/spin/Ry/cell) is larger than those in the high-density structures. This result suggests that the electronic states coming from the sp^3-hybridized atoms are more important for the superconductivity than those from the sp^2-hybridized atoms.

The proportion of the sp^3-originated electronic properties affects the superconducting properties even when the two structures have the same mass density. Figures 3(b) and 3(c) show the densities of states of boron-doped amorphous carbon with the same density of 3.0 g/cm^3 but with high [3.0(N)] and low T_c [3.0(I)], respectively. In the electronic structure of the 3.0(N), the contribution from the four-fold coordinated atom with energies near the Fermi energy is dominant because of its relatively high sp^3 proportion (71.9%). On the other hand, the contribution from four-fold and three-fold atoms are almost the same in the 3.0(I) structure. This larger contribution from four-fold coordinated atoms in the 3.0(N) should

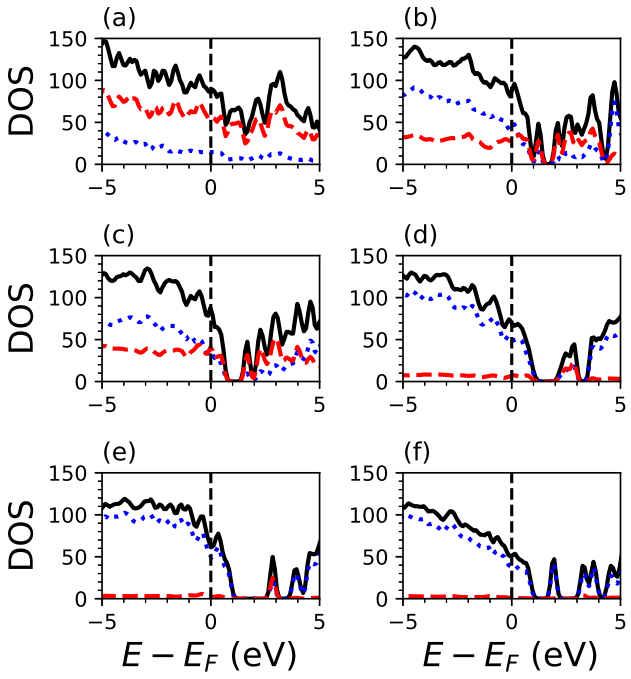

FIG. 3. (Color online) Electronic densities of states of boron-doped amorphous carbon with (a) 2.5(I), (b) 3.0(N), (c) 3.0(I), (d) 3.5(N) (e) 4.0(I), and (f) 4.5(N) structures. Black solid lines show the total densities of states. The partial density of states arising from three-fold and four-fold coordinated atoms are represented by red dashed and blue dotted lines, respectively. The vertical black dashed lines indicate the positions of the Fermi energy.

be a reason for the relatively higher transition temperature by 12 K.

Figure 4(a) shows the phonon density of states of boron-doped amorphous carbon. The low-density case [2.5(I), green solid line] exhibits more low frequency modes around 250 cm^{-1}. When the density is increased to 3.5 g/cm^3 [3.5(N), red dashed line], the low frequency modes decrease, and more phonon modes appear in the range between 750 to 1250 cm^{-1}. In addition, the high frequency modes above 1500 cm^{-1} almost disappear. However, the high frequency modes reappear when the density is further increased [blue dash-dotted line, 4.5(N)]. The phonon modes are stiffened due to the shortened bond lengths as described in Fig.2, caused by the extremely high density. The low-frequency modes become less dominant in higher density cases, indicating the blueshift of the entire spectrum from that of the 3.5(N) structure.

The Eliashberg spectral functions of boron-doped amorphous carbon are shown in

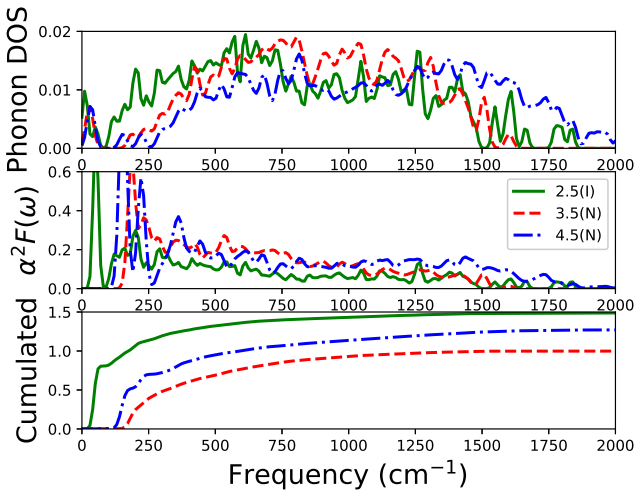

FIG. 4. (Color online) Phonon densities of states (top panel), Eliashberg spectral function (middle panel), and cumulated (integrated) contributions from Eliashberg spectral function to λ (bottom panel) of boron-doped amorphous carbon. Green solid, red dashed, and blue dash-dotted lines represent the 2.5(I), 3,5(N), and 4.5(N) cases, respectively. The phonon densities of states are normalized to one.

Fig. 4(b). The amplitude of the spectral function is low in the entire frequency region of the 2.5(I) structure (green solid line). The spectral function increases as a function of mass density. In general, the contribution from relatively low-frequency modes are dominant. However, the high frequency modes between 1500 and 1750 cm^{-1} interestingly contribute to the spectral function of the high-density 4.5(N) structure (blue dash-dotted line). These spectral weights appear because of the stiffening of phonon modes of the high-density amorphous carbon. The contribution from high-frequency modes is more favored for high T_c thorough a higher value of $\omega_{\log}$ (see Eq. 2). This indicates that a higher density can support a higher Tc through the increase of the phonon frequency and its logarithmic average.

In relatively low density of 2.5 and 3.0 g/cm^3 cases, three-fold and four-fold coordinated carbon atoms coexists. Here we analyze the contribution from atoms to the phonon modes of the 3.0(N) structure (phonon modes and Eliashberg spectral function are shown in the upper panel of Fig. 5). The lower panel of the Fig. 5 shows the norm of phonon eigenvectors ($\gamma_{\alpha,i}$) summed over three-fold (red open circles) and those from the four-fold (blue open

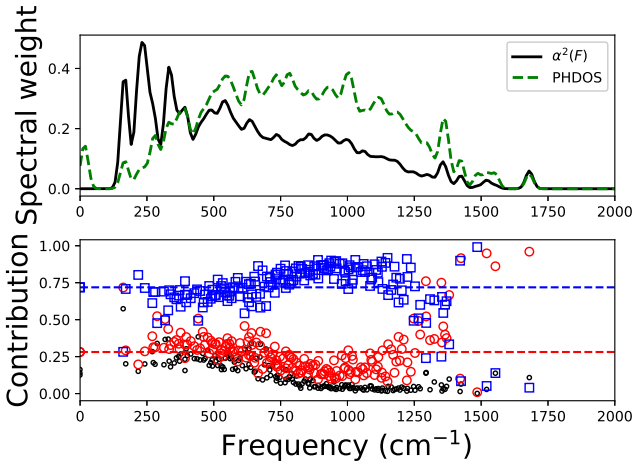

FIG. 5. (Color online) (Upper panel) Eliashberg spectral function (black solid line) and phonon density of states of 3.0(N) structure. Here the phonon density of states are multiplied by 30 to make it visible. (Lower panel) Norm of phonon eigenvectors ($\gamma_{\alpha,i}$) of the same structure summed over three-fold (open red circles) and four-fold (blue open squares) coordinated atoms. The horizontal red and blue dashed lines show the three-fold and four-fold proportion. Open black dots show the projection of the contribution from three-fold atoms onto out-of-plane motion.

squares) atoms. Here phonon eigenvectors must satisfy the normalization condition:

$$\sum_{\alpha,i} |\gamma_{\alpha,i}|^2 = 1. \tag{3}$$

Indices α and i represent atom index and Cartesian coordinate direction, respectively. Thus the sum of the red circle and the blue square for each mode should be equal to one. In the low-frequency region below 750 cm^{-1}, the red circles are mostly above the horizontal red dashed line, indicating more contribution from three-fold atoms than the actual proportion. On the other hand, the four-fold coordinated atoms contribute significantly to the middle-frequency range from 750 to 1250 cm^{-1}. The contribution from three-fold atoms is again dominant in the high frequency region above 1250 cm^{-1}. Therefore, the low and high frequency regions are dominated by the three-fold coordinated atoms whereas the middle-frequency modes are dominated by four-fold atoms.

The contribution from the three-fold coordinated atoms is further projected onto out-of-plane motion of carbon atoms (black open dots in Fig. 5). Here we first calculate the outer product of two bonding vectors for three-fold atoms. Then we take the inner product between

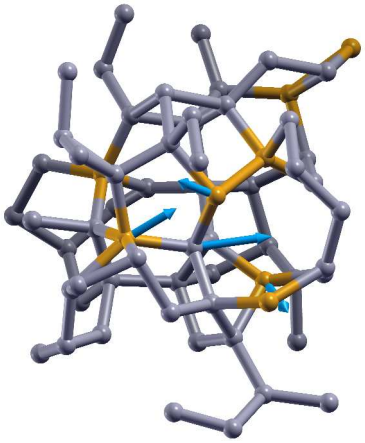

FIG. 6. (Color online) Eigendisplacement vectors (blue arrows) of the lowest optical phonon mode in 4.5(N) structure. Orange and gray spheres represent boron and carbon atoms, respectively.

phonon eigenvectors and the outer product to compute the projection. The projection indicates that the low-frequency modes below 1000 cm^{-1} mostly come from the out-of-plane motion of three-fold atoms. In contrast, there is virtually no contribution from the out-of-plane modes for high-frequency phonon modes. Instead, the high-frequency modes are mostly in-plane motion arising from the relatively strong sp^2 bonding.

In high-density cases, the analysis above is not meaningful because almost all atoms are four-fold coordinated or even five-fold coordinated. The phonon modes become stiff and the phonon DOS is blueshifted because of the high density. However, there are finite contributions from low-frequency modes to the Eliashberg spectral function. Figure 6 shows the eigendisplacement vectors of the lowest-frequency optical phonon mode in 4.5(N) structure. The leftmost arrow at the boron atom (orange sphere) points toward another boron atom with an arrow. The distance between these two boron atoms is 2.1 Å that is significantly shorter the second nearest-neighbor distance of diamond (2.5 Å). In fact, the second nearest-neighbor peak in the radial distribution function shifted toward short distance (see Fig. 2). Such a short distance under a high density and a highly disordered structure could soften phonon modes that contributes to the superconductivity.

V. SUMMARY

We have studied the superconducting properties of 12.5% boron-doped amorphous carbon with various mass densities. The electronic states of four-fold coordinated atoms to the density of states at the Fermi energy is important for a high superconducting transition temperature T_c. Thus low-density amorphous carbon is not suitable for high T_c because carbon atoms favor four-fold coordination for higher densities. A high-density amorphous carbon is therefore ore promising for a high T_c. In addition, there is the advantage arising from the stiffening of phonon modes. The highest T_c obtained in this work is 38 K, which is consistent with the previously reported theoretical and experimental studies [11, 13].

ACKNOWLEDGMENTS

YS and JRC acknowledge support from the U.S. Department of Energy (DoE) for work on nanostructures from grant DE-FG02-06ER46286, and on algorithms by a subaward from the Center for Computational Study of Excited-State Phenomena in Energy Materials at the Lawrence Berkeley National Laboratory, which is funded by the U.S. Department of Energy, Office of Science, Basic Energy Sciences, Materials Sciences and Engineering Division under Contract No. DE-AC02-05CH11231, as part of the Computational Materials Sciences Program. Computational resources are provided in part by the National Energy Research Scientific Computing Center (NERSC). MLC acknowledges support from the National Science Foundation Grant No. DMR-1508412 and from the Theory of Materials Program at the Lawrence Berkeley National Lab funded by the Director, Office of Science and Office of Basic Energy Sciences, Materials Sciences and Engineering Division, U.S. Department of Energy under Contract No. DE-AC02-05CH11231. MLC acknowledges useful discussions with Professor Jay Narayan.

---

[1] E. A. Ekimov, V. A. Sidorov, E. D. Bauer, N. N. Mel'nik, N. J. Curro, J. D. Thompson, and S. M. Stishov, Nature (London) **428**, 542 (2004).

[2] Y. Takano, T. Takenouchi, S. Ishii, S. Ueda, T. Okutsu, I. Sakaguchi, H. Umezawa, H. Kawarada, and M. Tachiki, Diamond and related materials **16**, 911 (2007).

[3] H. Okazaki, T. Wakita, T. Muro, T. Nakamura, Y. Muraoka, T. Yokoya, S. Kurihara, H. Kawarada, and T. Oguchi, Appl. Phys. Lett. **106**, 052601 (2015).

[4] N. Murata, J. Haruyama, J. Reppert, A. M. Rao, T. Koretsune, S. Saito, and Y. Matsudaira, M. abd Yagi, Phys. Rev. Lett. **101**, 027022 (2008).

[5] J. Haruyama, M. Matsudaira, J. Reppert, A. Rao, T. Koretsune, S. Saito, H. Sano, and Y. Iye, J. Supercond. Nov. Magn. **24**, 111 (2011).

[6] K. Tanigaki, T. W. Ebbesen, S. Saito, J. Mizuki, and J. S. Tsai, Nature (London) **352**, 222 (1991).

[7] T. E. Weller, M. Ellerby, S. S. Saxena, R. P. Smith, and N. T. Skipper, Nature Phys. **1**, 39 (2005).

[8] Y. Cao, V. Fatemi, S. Fang, K. Watanabe, T. Taniguchi, E. Kaxiras, and P. Jarillo-Herrero, Nature **556**, 43 (2018).

[9] J. Narayan and A. Bhaumik, J. Appl. Phys. **118**, 215303 (2015).

[10] A. Bhaumik, R. Sachan, S. Gupta, and J. Narayan, ACS Nano **11**, 11915 (2017).

[11] A. Bhaumik, R. Sachan, and J. Narayan, ACS Nano **5351**, 11 (2017).

[12] J. Nagamatsu, N. Nakagawa, T. Muranaka, Y. Zenitani, and J. Akimitsu, Nature (London) **410**, 63 (2001).

[13] Y. Sakai, J. R. Chelikowsky, and M. L. Cohen, Phys. Rev. B **97**, 054501 (2018).

[14] M. L. Cohen, Phys. Scr. **T1**, 5 (1982).

[15] J. Ihm, A. Zunger, and M. L. Cohen, J. Phys. C **12**, 4409 (1979).

[16] N. Troullier and J. L. Martins, Phys. Rev. B **43**, 1993 (1991).

[17] P. Hohenberg and W. Kohn, Phys. Rev. **136**, 864 (1964).

[18] W. Kohn and L. J. Sham, Phys. Rev. **140**, 1133 (1965).

[19] D. M. Ceperley and B. J. Alder, Phys. Rev. Lett. **45**, 566 (1980).

[20] J. P. Perdew and A. Zunger, Phys. Rev. B **23**, 5048 (1981).

[21] J. R. Chelikowsky, N. Troullier, and Y. Saad, Phys. Rev. Lett. **72**, 1240 (1994).

[22] J. R. Chelikowsky, J. Phys. D **33**, R33 (2000).

[23] L. Kronik, A. Makmal, M. L. Tiago, M. M. G. Alemany, M. Jain, X. Huang, Y. Saad, and J. R. Chelikowsky, Phys. Status Solidi B **243**, 1063 (2006).

[24] A. Natan, A. Benjamini, D. Naveh, L. Kronik, M. L. Tiago, S. P. Beckman, and J. R. Chelikowsky, Phys. Rev. B **78**, 075109 (2008).

[25] R. Biswas and D. R. Hamann, Phys. Rev. B **34**, 895 (1986).

[26] S. Baroni, S. de Gironcoli, A. dal Corso, and P. Giannozzi, Rev. Mod. Phys. **73**, 515 (2001).

[27] P. Giannozzi, S. Baroni, N. Bonini, M. Calandra, R. Car, C. Cavazzoni, D. Ceresoli, G. L. Chiarotti, M. Cococcioni, I. Dabo, A. Dal Corso, S. de Gironcoli, S. Fabris, G. Fratesi, R. Gebauer, U. Gerstmann, C. Gougoussis, A. Kokalj, M. Lazzeri, L. Martin-Samos, N. Marzari, F. Mauri, R. Mazzarello, S. Paolini, A. Pasquarello, L. Paulatto, C. Sbraccia, S. Scandolo, G. Sclauzero, A. P. Seitsonen, A. Smogunov, P. Umari, and R. M. Wentzcovitch, J. Phys. Condens. Matter **21**, 5502 (2009).

[28] F. Giustino, Rev. Mod. Phys. **89**, 015003 (2017).

[29] P. B. Allen and R. C. Dynes, Phys. Rev. B **12**, 905 (1975).

[30] Y. Sakai, J. R. Chelikowsky, and M. L. Cohen, Phys. Rev. Mater. **2**, 074403 (2018).